Kristin M. Riching,[†‡] Benjamin Cox,[§] Max R. Salick,[¶||] Carolyn Pehlke,[‡] Andrew S. Riching,[**] Benjamin R. Bass,[††] Wendy C. Crone,[||] Yi Jiang,[‡‡] Alissa Weaver, [§§] Kevin W. Eliceiri, [‡†§¶¶] and Patricia J. Keely[‡¶¶||||*]

3D collagen alignment enhances breast cancer cell persistence and limits protrusions

SUPPLEMENTARY MATERIAL

This file contains the following items:

1. Supplementary Materials and Methods
2. Supplementary legends for Movies S1, S2, and S3
3. Supplementary Figure S1, Figure S2, and Figure S3
4. Supplementary Table S1

† Biomedical Engineering Program, University of Wisconsin, Madison, Wisconsin 53706,
‡ Laboratory for Optical and Computational Instrumentation, University of Wisconsin, Madison, Wisconsin 53706,
§ Department of Medical Physics, University of Wisconsin, Madison, Wisconsin 53706,
¶ Materials Science Program, University of Wisconsin, Madison, Wisconsin 53706,
|| Department of Engineering Physics, University of Wisconsin, Madison, Wisconsin 53706,
** Department of Cell and Regenerative Biology, University of Wisconsin, Madison, Wisconsin 53706
†† Saris Cycling Group, Madison, Wisconsin, 53711,
‡‡ Department of Mathematics and Statistics, Georgia State University, Atlanta, Georgia 30303,
§§ Department of Cancer Biology, Vanderbilt University Medical Center, Nashville, Tennessee 37232,
¶¶ Department of Cell and Regenerative Biology, University of Wisconsin, Madison, Wisconsin 53706, and
|||| University of Wisconsin Paul P. Carbone Comprehensive Cancer Center, University of Wisconsin, Madison, Wisconsin 53706,

Supplementary Materials and Methods

Reagents and chemicals

Type I rat tail collagen was obtained from BD Biosciences (San Jose, CA). DMEM cell culture media was purchased from Life Technologies (Grand Island, NY) and fetal bovine serum was purchased from Gemini Bio-Products (West Sacramento, CA). MDA-MB-231 epithelial cells were obtained from ATCC (Manassas, VA). Phospho-MLC antibody was purchased from Cell Signaling Technology (Danvers, MA). The ROCK inhibitor H1152 and the MLCK inhibitor ML-7 were purchased from EMD Millipore (Darmstadt, Germany).

Cell culture and transfection

MDA-MB-231 cells were maintained in DMEM with 10% serum in a 37°C incubator with 5% CO_2. Lentiviral Lifeact-mRFP constructs were a kind gift from Maddy Parsons (King's College London, London, UK). Phoenix (HEK293) cells were obtained from the National Gene Vectro Biorepository (Indianapolis, IN) and used for lentiviral production as described (1). Cells were removed from culture dishes with 0.05% trypsin and centrifuged at 300 × *g* for 3 min to remove trypsin prior to addition of neutralized collagen solution for culture in 3D collagen gels.

Mechanical alignment of collagen gels

A device to mechanically strain dogbone-shaped collagen gels was modeled in SolidWorks (Daussalt Systemes, Waltham, MA) and 3D-printed. The device was based on a design by Vader et al. (2), and consisted of a micrometer that drove and accurately recorded displacements of one of two pins that contacted pieces of polypropylene mesh embedded in the gel. The device was mounted to a 3D printed stage designed to fit a multiphoton microscope. Dogbone-shaped collagen gels were pre-strained to 30% using this strain device prior to mechanical testing and were either left unfixed or were fixed with 4% paraformaldehyde for 10 minutes.

To strain larger collagen dogbone-shaped specimens, a weight-based loading system was used. This system consisted of a set of grips where one grip remained stationary and the other was pulled horizontally by a cable attached to a series of weights hung over a pulley. Both grips containing the collagen gel were immersed in a bath of PBS and the gel was strained to 30%, after which the gel was fixed with 4% paraformaldehyde for 10 minutes. The gel was then removed from the grips and a 3D-printed cutter in the shape of a dogbone was used to cut specimens either parallel or perpendicular to the direction of the applied strain. Grip sections of the cut specimens were carefully sandwiched between pieces of polypropylene mesh to facilitate handling.

3D printing

Several components of the collagen strain device were fabricated using three-dimensional (3D) printing techniques. The stage of the strain device was made using a Dimension Elite 3D Printer (Stratasys Ltd., Rehovot, Israel). This machine creates plastic parts using the process of fused deposition modeling (FDM). The arm that held the stationary pin and the arm that connected to the micrometer in the strain device were fabricated using a Viper Si2 3D Printer (3D Systems inc., Rock Hill, SC). This machine creates parts using the process of stereolithography (SL). Both of these processes have been previously described (3).

Mechanical testing of collagen

Collagen gels were prepared by neutralizing acid-soluble rat-tail collagen with 100mM HEPES buffer in 2x PBS in a 1:1 ratio, and then diluted with DMEM to obtain the final collagen concentration as described in Wozniak et al. (4). Neutralized collagen was then poured into a stainless steel mold in the shape of a dogbone with dimensions taken from Roeder et al. (5). These dimensions consisted of a 10mm long by 4mm wide and approximately 1mm thick gauge region, and 10mm long by 20mm wide grip sections. Pieces of polypropylene mesh were embedded into the grip sections of the dogbone to facilitate removal from the mold and to ensure adequate sample gripping for mechanical testing. Gels were left undisturbed at room temperature until gels were visibly opaque, then stored in a 37°C incubator to complete polymerization overnight. The cross-sectional area of the dogbone gauge region was measured using digital calipers to measure the width, and optical sectioning by second harmonic imaging and a 10x objective to measure gel thickness. Tensile testing was performed using a similar procedure as Lopez-Garcia et al. (6). Briefly, a vertical-loading Instron 5548 MicroTester with a 10 N load cell and a crosshead displacement rate of 1mm/min was used. Samples loaded into the grips of the Instron were then immersed in a PBS-filled custom water-jacketed Pyrex environmental chamber heated to 37°C with a PolyScience digital temperature controller heater/circulator for the duration of the test. Load data was acquired using Merlin v5.04 software. 1μm glass beads were deposited on the surface of collagen specimens and imaged every 10 seconds using a Photometrics MicroPublisher 5.0 RTV and QCapture Pro 5.1.1.14 acquisition software. All samples were strained until failure, and samples where failure occurred prematurely at the grip sections were discarded. The effect of buoyancy on the load cell was measured by conducting an identical test without the specimen for all measured specimens, and subtracted from the data to obtain the load incurred by the collagen alone. Strain analysis was conducted in FIJI by measuring the relative displacement of glass beads. Sample strain was computed as a ratio of the change in distance between bead pairs to their initial separation. Load per unit area was calculated, and resulting stress-strain plots were generated in MATLAB (MathWorks, Natick, MA).

Multiphoton SHG imaging and CurveAlign analysis

Collagen gels were imaged via second harmonic generation (SHG), a technique that employs multiphoton microscopy to allow visualization of non-centrosymmetric molecules independent of fluorescence. Acquisition was conducted on WiscScan software and a Nikon 40x Apo water immersion lens (Numerical Aperture, N.A. 1.15 and Working Distance, W.D. 0.61) was used to visualize the organization of individual fibers in the matrix. Z-stacks consisting of an inter-plane spacing of no more than 10μm were collected to obtain an accurate depiction of fiber organization across gel thickness for collagen gels submitted for tensile testing and for collagen in microchannels. Images of collagen fibers were analyzed using CurveAlign software (www.loci.wisc.edu/software/curvelet-based-alignment-analysis) to measure the 2D-projected angles of all fibers relative to the horizontal, and to obtain a coefficient of alignment.

Microchannel migration assay

Microchannels with widths of 1mm and 3mm were fabricated using soft lithography according the protocol described in Sung, et al. (7). Briefly, SU8-100 was spun onto a silicon wafer to obtain a mold with channel thickness of 200μm. After UV exposure of the first layer, a second SU8-100 layer was spun to obtain a 200μm port layer. Polydimethylsiloxane (PDMS, Sylgard

184 Silicon Elastomer Kit, Dow Corning, Midland, MI) was molded over the master, and cured PDMS channels were adhered to glass bottom culture dishes (MatTek, Ashland, MA).

PDMS microchannels with the center cell port initially covered with a thin PDMS rectangle were first coated with 50μg/ml collagen in water for 1-2 hours, and then washed three times with PBS. Neutralized collagen solution containing penicillin/streptomycin was prepared and a droplet of 100-200μL was added to the flow inlet ports of the channels. The channels were then immediately placed at 4°C for overnight incubation to slow the polymerization kinetics and allow nucleation of short fibers (7). Immediately following incubation, a vacuum was applied to the outlet ports of wide channels to allow flow of collagen through the channels. After 2-3 minutes at room temperature, vacuum was applied to narrow channels to induce flow of collagen. An additional 2-3 minutes after collagen flow, thin PDMS rectangles were used to carefully cover both the inlet and outlet channel ports, after which the center cell port was uncovered. Covering the inlet and outlet ports prior to uncovering the center port allowed for minimal additional flow of collagen when center port was uncovered and cells added. A 1.5μL cell suspension of 5×10^6 cells/ mL was added to the center port. Channels were left undisturbed at room temperature for an additional 5 minutes, then placed in 37°C incubator for 10 minutes. All PDMS rectangular covers were removed and 2.5mL DMEM was added to the dish. For endpoint analysis, cells were allowed to migrate into channels for three days, then fixed with 4% paraformaldehyde for 10 minutes and then nuclei were stained with bis-benzimide. For time-lapse experiments, cells were imaged 2-3 days after they began migrating into the channels from the port. DMEM was replenished the night before imaging. For inhibitor experiments, either H1152 or ML-7 was added at a final concentration of 10μM or 2μM, respectively 30 minutes prior to imaging.

Confocal imaging

Channels for end point and time-lapse experiments were imaged using a Prairie Technologies point scanning inverted confocal microscope with PrairieView acquisition software (Prairie Technologies, Middleton, WI). A Nikon 10x Plan Fluor objective (N.A. 0.3 and W.D. 16) and 405nm laser line were used to image bis-benzimide stained nuclei, and serial images of cells that migrated out of the port were collected that were later compiled into montages of 3-9 images using a stitching algorithm in FIJI (8). For time-lapse experiments, DIC imaging combined with the 488nm laser line were used to image MDA-MB-231 cells and FITC-collagen, respectively. To observe cell migration, a Nikon 20x Plan Apo VC objective (N.A. 0.75 and W.D. 1) was used to collect images every 10 minutes for a period of 6 hours. To observe fiber displacement, a 20x objective with an optical zoom of 3 was used to collect images every 4 minutes for 2 hours. To observe cellular protrusions containing Lifeact-mRFP, a 20x objective with optical zoom of 3 and 561nm laser line was used to collect images every 4 minutes for 40 minutes. For all live imaging, a LiveCell (Pathology Devices, Westminster, MD) environmental chamber was used to maintain a constant 37°C, 5% CO_2, and 75% humidity for the duration of the experiment.

Cell migration analysis

For channel endpoint analysis, images were compiled into montages of 3-9 images using a stitching algorithm in FIJI. Nuclear stained images were segmented using the Yen algorithm and converted into a binary image for a nuclear object count. Bright field images of each channel were used to generate masks of 100μm-wide concentric rings surrounding the port, which were

intersected by the channel walls. Masks were applied to the montages containing the stained nuclei, and nuclei were counted using the 3D object counter plugin in FIJI. Nuclear counts were compiled and normalized to the area of the ring in which they were counted.

For time-lapse migration analysis, cells were tracked using the MTrackJ plugin in FIJI, and all x-y positions at each time point were recorded. Only individual cells were included in the analysis to eliminate confounding data from cell-cell interactions or collective migration. In some cases, a small, but significant amount of image drift occurred in the x-y plane. To compensate for this, a fiduciary marker in the form of a particle > 100μm from the nearest cell, or region of the channel wall or port was tracked for all images collected. The image drift was then computed and subtracted from the positions of each cell in the image. Only cells that remained in the field of view for the entire experiment were analyzed, and non-motile or dividing cells were excluded. A non-motile cell was defined as one that did not translocate more than one cell length in distance, or about 20μm for the duration of the time-lapse. For experiments involving the ROCK inhibitor, H1152, very little to no migration was observed. In order to maintain consistency in the numbers of cells analyzed per image, the percentage of cells that corresponded to the motile fraction (about 65% of cells in each image) of untreated cells was used to analyze images of H1152 treated cells.

Cell position data was then used to calculate speed and persistence. Speed was computed as the total track length divided by time, and therefore represented an average speed over the entire track. Direction-dependent speed in narrow channels was not measured as the tracks were predominantly parallel to the direction of alignment. Chemotactic index, given by: $CI = \left(\frac{Net\ Displacement}{Total\ Track\ Length}\right) \cos\alpha$, was used as a measure of cellular persistence relative to the orientation of aligned collagen. Measurements were made over the same interval of time to normalize the time component of *CI*. In the expression of CI, α represents the angle between the net migration vector and the channel wall, which corresponds to the direction of alignment in narrow channels. In order to account for the observation that more cells in narrow channels often reversed direction multiple times along aligned collagen fibers, which would have a significant effect on the magnitude of their net migration vector, the absolute value of all net displacements for cells in both narrow and wide channels was used to compute *CI*.

Collagen fiber tracking analysis

Images of FITC-labeled collagen fibers were analyzed in FIJI using the MTrackJ plugin. Fiber junctions or regions of fibers that were clearly present in all images were used for tracking. Image drift was calculated in a similar fashion to the migration analysis by tracking either a stationary collagen fiber at least 50μm away from the nearest cell, or a stationary object in the corresponding bright field image. Fiber positions were calculated by subtracting the image drift, and a sum total of the fiber displacement for the duration of the 2-hour imaging experiment was computed.

2D migration experiments on polyacrylamide gels

Cell migration experiments on 2D polyacrylamide (PA) gels were carried out according to other reports (9-11). The amount of added bis-acrylamide cross-linker resulted in PA gels of different stiffness. The 10KPa and 44KPa gel stiffness conditions were chosen to correspond to the measured moduli of unfixed 1mg/ml and 4mg/ml collagen gels from Roeder et al. (5). A

100KPa condition was also added to correspond to the estimated modulus of an unfixed aligned 4mg/ml collagen gel. The ratio of acrylamide to bis-acrylamide for gels of different stiffness was calculated from (9). PA gels were further cross-linked with sulfo-SANPAH (Pierce) under UV for 90 seconds, and 500μL of a 200μg/mL collagen in water solution was added to the gels for 2 hours at room temperature. For experiments where collagen concentration was varied instead of gel stiffness, 10KPa gels were used and collagen concentrations of 50μg/mL and 400μg/mL were added to the gel. Gels were carefully rinsed with PBS three times and sterilized under UV for 30 minutes. 10,000 MDA-MB-231 cells were seeded onto the surface of PA gels and allowed to adhere overnight. Confocal time-lapse experiments of migrating cells were conducted the following day.

Cell migration model

A computational model of cell migration as a function of time was developed using MATLAB (MathWorks). To correspond to the 2D measurements of cell migration in 3D narrow and wide microchannels, cell displacements were computed in one plane from an initial random generation of protrusion vector magnitudes, P, and orientations, θ. Cells were defined to contain up to 30 arbitrary protrusion vectors to simulate the likely opposing forces produced from pseudopods and associated adhesions (12). Protrusion vectors were therefore limited to defined orientations or "slots" in 12° increments, or 360°/30, distributed around the cell. At each time step, the magnitudes and protrusion vector slot orientations were randomly determined. A vector sum was then computed, which resulted in the distance traveled by the cell at that time step. To simulate the observation that cellular adhesions are stabilized and likely maintained by mechanical force (13), we used a threshold for protrusion vector magnitudes to allow the orientations of some vectors to persist into the next time step. Vectors with magnitudes above the threshold (85% of vectors), maintained their orientations for the next time step, while vectors with magnitudes below the threshold (15% of vectors) had their orientations re-randomized for the next time step. This allowed representation of both stabilized and dynamic protrusions, resulting in the simulated cells making several persistent consecutive moves, and less dramatic changes in direction to better correspond with our observations in 3D collagen gels. All protrusion vector magnitudes were re-randomized at every time step.

With this simplified model of randomly generated protrusion vector magnitudes and orientations, we varied the number of protrusion vectors and computed the resulting cell speed over 36 time steps. The model produced a bimodal relationship between speed and the number of protrusion vectors (Figure S2 *A*). This initial result mimics the biphasic nature of migration speed with integrin expression (14), and serves to validate our approach of using randomized protrusion vectors to simulate cell movement.

In order to make comparisons of cell migration in 3D matrices with varying physical and mechanical properties, we incorporated model coefficients to represent matrix stiffness, ligand density, and alignment that were defined to be dependent on the measured experimental conditions. These coefficients were then used to modify the components of the protrusion vectors prior to the computed vector sum at each time step. Equations for the parallel and perpendicular components of the matrix-modified protrusion vectors ($P_{M_\parallel}$ and $P_{M_\perp}$) with respect to the direction of alignment are given by:

$$P_{M_\parallel} = P_\parallel \left(\frac{C_S}{C_{LD}(1-C_A)}\right) \text{ and } \quad P_{M_\perp} = P_\perp \left(\frac{C_S(1-C_A)}{C_{LD}}\right)$$

where C_S is the coefficient of matrix stiffness, C_A is the model coefficient of alignment, and C_{LD}, is the coefficient of ligand density. As C_A approached zero, representing a random matrix, equations for $P_{M_\parallel}$ and $P_{M_\perp}$ reduced to an identical expression, one that was only dependent on matrix stiffness and ligand density.

Relationships for the model coefficients and the measured experimental conditions are shown in Fig. S2 *B-D*, and were determined using an iterative approach that consisted of varying each parameter independently to determine the effects on the others. Additionally, the number of protrusion vectors was assumed to depend on alignment and ligand density (Fig. S2 *E*) and was computed for each set of matrix conditions.

To better model the increased cellular persistence seen with increasing matrix alignment, we incorporated a probability that cells will continue in their initial randomly determined direction as a function of increasing alignment. We computed the protrusion vector orientation slot that was nearest the cell's net displacement vector at each time step. All floating vectors had a greater probability of either falling within this slot, or the nearest 3 slots on either side of it unless they were already occupied. If all of these "persistent" slots were filled, remaining vectors were randomly assigned to any open slot around the cell. The probability of filling persistent slots increased as a linear function of C_A, and increased cellular persistence was simulated in this way at every time step.

All model parameters used are tabulated in Table S1.

Protrusion analysis

Time-lapse confocal images (Fig. *S3A*) were thresholded in FIJI using the Huang algorithm (Fig. *S3B*) and analyzed for number and length of protrusions at each time point using custom MATLAB code. For each cell, the locations of the centroids and boundary pixels were identified. From the boundary pixels, the perimeter was determined, and the number of equally spaced perimeter nodes was defined as a linear function of perimeter. This ensured that cells having different perimeters would have similar perimeter node spacing. Once the perimeter nodes were determined, sharp convex regions in boundary curvature were identified by summing the exterior angles of the 5 subsequent nodes at each node of the enclosed polygon. Any sum of five nodes that resulted in an angle greater than 105° was considered a convex region. Where there were consecutive nodes with sums greater than this threshold, the algorithm searched for the position of the starting node that resulted in the greatest sum. The tip of the protrusion was then determined by finding the maximum external angle formed between any three nodes within the identified convex region. Finally, in order to better distinguish between protrusions and regions of the cell that were only moderately convex, the smallest circle containing the tip of the protrusion and the adjacent two nodes on either side was computed. If the radius of the circle was greater than 2μm, the convex region was not counted as a protrusion. All boundary nodes and identified protrusions were overlaid onto all thresholded images of cells (Fig. *S3C*) and lengths of protrusions relative to the cell centroid were computed. In order to determine the accuracy of the algorithm at identifying protrusions, 5 panelists were given 26 thresholded images of cells and asked to identify all protrusions. Tested against the results from the panelists, the algorithm identified protrusions for each cell that fell within the range of responses

on average 93% of the time. All cells imaged in both narrow and wide channels were then analyzed using this approach.

Statistics

All statistics were computed using a two-sided Wilcoxon Rank Sum test using Mstat software (McArdle Laboratory for Cancer Research, Madison, WI). Differences in the data were deemed significant if a P-value < 0.05 was obtained. All significant differences were denoted with an asterisk (*) in the corresponding figures.

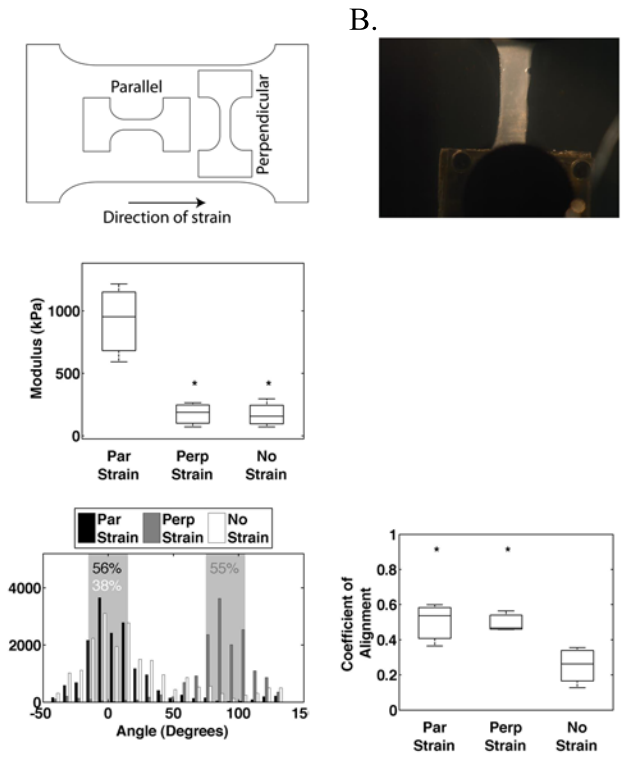

Figure S1. Aligned collagen is stiffest along the axis of alignment. *(A)* Diagram of test conditions. Large collagen dogbone gels are cast and subjected to 30% strain. After fixing with 4% PFA, two dogbone test specimens are cut parallel and perpendicular to the strained axis. *(B)* Image of gauge region of dogbone-shaped collagen gel in one grip of the Instron. Extreme care was taken to load gels into grips without damaging gels. *(C)* Tensile modulus of unstrained, parallel strained and perpendicular strained gels fixed with PFA, n=3 gels, $p < 0.05$. *(D, left)* Histograms of fiber angles generated from CurveAlign software of unstrained, parallel strained *(Par Strain)*, and perpendicular strained *(Perp Strain)* gels. Percentages represent the fraction of fiber angles ±15° from 0° and 90° *(shaded regions)*. *(D, right)* Coefficient of alignment of unstrained, parallel strained, and perpendicular strained gels, n=3, $p < 0.05$.

Fig. S2

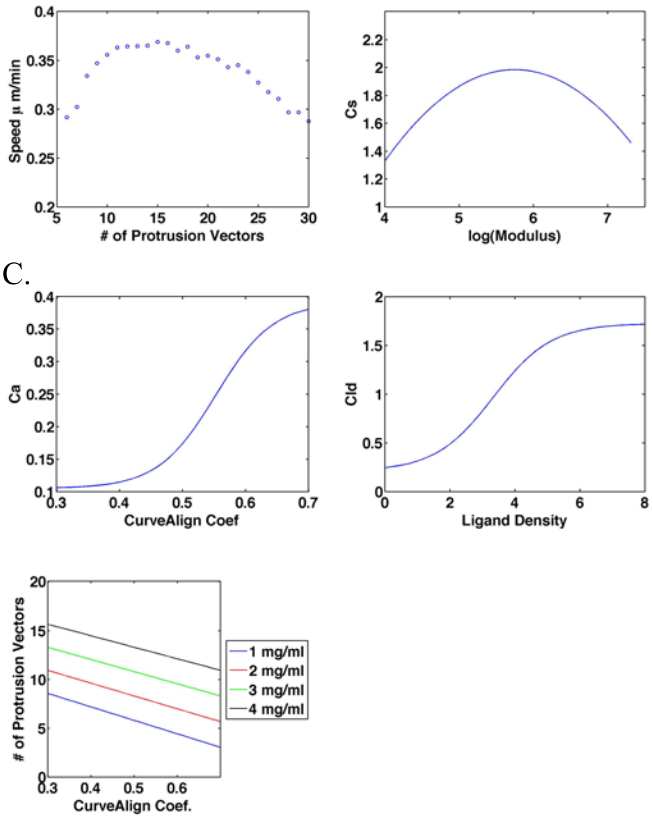

Figure S2. Migration model coefficient relationships. *(A)* Model predicts migration speed is biphasic with the number of cell protrusion vectors. *(B)* Model relationships between experimental conditions and model coefficients for Coefficient of Stiffness, *(C)* Coefficient of Alignment, and *(D)* Coefficient of Ligand Density. *(E)* Model relationship showing a linear dependence of the number of protrusion vectors on alignment for various collagen densities.

Table S1

Model Parameters	Variable Name	Value(s)
Protrusion vector	P	0 – 0.7
Vector orientation slot	θ	(12 – 30) × 12°
Vector threshold	Th	0.15 × PV
Stiffness	S	70 – 1000
Coefficient of stiffness	C_S	1.5 – 2
CurveAlign coefficient	A	0.3 – 0.7
Coefficient of alignment	C_A	0.1 – 0.4
Ligand density	LD	1 – 4
Coef. of ligand density	C_{LD}	0.25 – 1.25
# of protrusion vectors	N_P	3 – 27

Table S1. Migration model input parameters. Values and ranges are listed for all input parameters used in the model.

C.

Figure S3. Cell protrusion analysis. *(A)* Confocal images of MDA-MB-231 cells expressing Lifeact-mRFP in narrow *(left panel)* and wide *(right panel)* channels. *(B)* Thresholded images and *(C)* output images from custom MATLAB code showing the equally spaced nodes on the cell boundary *(blue circles)* and the number and location of identified protrusions *(red circles)*.

Movie S1. 6-hour confocal time-lapse images of MDA-MB-231 cells migrating in wide (*top panels*) and narrow (*bottom panels*) microchannels. DIC images (*left panels)* and fluorescence

images of FITC-labeled collagen fibers (*right panels*) were collected at 10-minute intervals, scale bar, 500μm.

Movie S2. 2-hour confocal time-lapse images of MDA-MB-231 cells displacing collagen fibers in wide (*top panels*) and narrow (*bottom panels*) microchannels. DIC images (*left panels)* and fluorescence images of FITC-labeled collagen fibers (*right panels*) were collected at 4-minute intervals, scale bar, 200μm.

Movie S3. 40-minute confocal time-lapse images of MDA-MB-231 cells expressing Lifeact-mRFP to visualize protrusions in narrow *(top)* and wide *(bottom)* microchannels. Scale bar, 20μm.

Matlab code for model of cell migration in aligned collagen

```
% Cell Migration Parameter Model

% 3D cell migration is modeled by measureable inputs: Vc = discrete cell
% displacement, A = collagen alignment, Ld = ligand density, S = collagen
% matrix stiffness; unknown inputs dependent on measureable inputs: Cs =
% stiffness coefficient, Cc = confinement coefficient (inverse of porosity), GH = number of
% protrusion vectors per cell, Ca = alignment coefficient; and random inputs:
% Theta = random initial direction of grappling hook, Vh = random magnitude
% of pull per protrusion vector

%%% Model Inputs

t=36; % Number of time points
n=100;  % Number of iterations
int = 10;   % Time interval (in minutes)
Vcmax = .7;
Vcmin = 0.15*Vcmax;

%%% Empirically determined model relationships

Sa = 1000;   % alignment modulus in KPa
Sr = 225;   % random modulus in KPa ~ perpendicular modulus

y03 = -5.1136;
a3 = 2.469;
b3 = -.2147;

Csa = y03 + a3*log(Sa) + b3*log(Sa)^2;
Csr = y03 + a3*log(Sr) + b3*log(Sr)^2;

Aa = 0.7; % From CurveAlign analysis
Ar = 0.3;
Ar0 = 0;
```

```
a = .2868;
b = .0457;
x0 = .5526;
y0 = .1047;
Ca = y0 + a/(1+exp(-(Aa-x0)/b));
Cr = y0 + a/(1+exp(-(Ar-x0)/b));
Cr0 = y0 + a/(1+exp(-(Ar0-x0)/b));

Ld =4;  % in mg/ml
y01 = .2096;
x01 = 3.3376;
a1 = 1.5142;
b1 = .8909;
Ccld  = y01 + a1/(1+exp(-(Ld-x01)/b1));

GHa = round((.6667*Ld-14.4667)*Aa+(2.1667*Ld+10.5333))
GHr = round((.6667*Ld-14.4667)*Ar+(2.1667*Ld+10.5333))

proba = [.5+(Ca-Cr0) .5-(Ca-Cr0)]
probr = [.5+(Cr-Cr0) .5-(Cr-Cr0)]

%%% Aligned Case

Dx=zeros(t,n);
Dy=zeros(t,n);
X=zeros(t,n);
Y=zeros(t,n);
R=zeros(t,n);
alpha=zeros(t,n);

for k=1:n

   nearRslots = 0;
   Thetapos = randperm(30)';
   Theta = Thetapos(1:GHa).*12;

   for i=1:t

      Vh = rand(GHa,1)*Vcmax;
      Vhx = Vh.*cos(Theta.*pi/180);
      Vhy = Vh.*sin(Theta.*pi/180);
      Fx = Vhx.*Csa*1/(Ccld*(1-Ca));
      Fy = Vhy.*Csr*(1-Ca)/Ccld;
      Rx=0;
      Ry=0;
      Thetanew=zeros(GHa,1);
```

```
for j=1:GHa

   Rx=Rx+Fx(j);
   Ry=Ry+Fy(j);

   if Vh(j) >= Vcmin

      Thetanew(j)=Theta(j);
   end
end

Dx(i,k)=Rx;
Dy(i,k)=Ry;
R(i,k)=sqrt(Rx^2+Ry^2);
alpha(i,k)=atan(Ry/Rx)*180/pi;

if Rx < 0 && Ry > 0
   alpha(i,k) = alpha(i,k) + 180;
elseif Rx < 0 && Ry < 0
   alpha(i,k) = alpha(i,k) + 180;
elseif Rx > 0 && Ry < 0
   alpha(i,k) = alpha(i,k) + 360;
end

Alpha = alpha(i,k);
slotdir = 12:12:360;
Rslot = find((slotdir < Alpha & slotdir > Alpha-6) | (slotdir > Alpha & slotdir < Alpha+6));
newGH = length(find(Thetanew==0));
nearRslots = Rslot*12-3*12:12:Rslot*12+3*12;

openslots = find(ismember(nearRslots,Thetanew)==0);
openslotdir = nearRslots(openslots);

if length(newGH)>length(openslotdir) && newGH ~=0
   Thetanew = [Thetanew; openslotdir'];
elseif length(newGH)<length(openslotdir) && newGH ~=0
   slotprob=[ones(length(openslotdir),1).*proba(1)/length(openslotdir);proba(2)];
   for q=1:length(newGH)
      r=rand;
      x = sum(r >= cumsum([0; slotprob]));
      for z=1:length(openslotdir)
         if z==x
            Thetanew=[Thetanew; openslotdir(z)];
         end
      end
```

```
        end
    end

    Thetanew(Thetanew==0)=[];
    thetanew=Thetanew./12;
    newThetapos = randperm(30)';
    norepeats=find(ismember(newThetapos,thetanew)==0);
    newThetapos=newThetapos(norepeats);
    if GHa-length(Thetanew) == 0
        Theta = Thetanew;
    else
        T = newThetapos(1:GHa-length(Thetanew)).*12;
        Theta=[Thetanew; T];
    end

  end

  for i=2:t+1

    X(i,k) = Dx(i-1,k)+X(i-1,k);
    Y(i,k) = Dy(i-1,k)+Y(i-1,k);

  end

end

NetDispA = sqrt((X(size(X,1),:)-X(1,:)).^2+(Y(size(Y,1),:)-Y(1,:)).^2);
SpeedA = sum(R,1)/(t*int);

AbsNetAlphaa = atan(sum(abs(Dy))./sum(abs(Dx)));

CIa = sqrt((sum(abs(Dx))).^2+(sum(abs(Dy))).^2)./sum(R).*cos(AbsNetAlphaa);

%%% Random Case

Dx=zeros(t,n);
Dy=zeros(t,n);
X=zeros(t,n);
Y=zeros(t,n);
R=zeros(t,n);
alpha=zeros(t,n);

for k=1:n

  nearRslots = 0;
  Thetapos = randperm(30)';
```

```
Theta = Thetapos(1:GHr).*12;

for i=1:t

    Vh = Vcmax*rand(GHr,1);
    Vhx = Vh.*cos(Theta.*pi/180);
    Vhy = Vh.*sin(Theta.*pi/180);
    Fx = Vhx.*Csr*1/(Ccld*(1-Cr));
    Fy = Vhy.*Csr*(1-Cr)/Ccld;
    Rx=0;
    Ry=0;
    Thetanew=zeros(GHr,1);

    for j=1:GHr

        Rx=Rx+Fx(j);
        Ry=Ry+Fy(j);

        if Vh(j) >= Vcmin

            Thetanew(j)=Theta(j);
        end
    end

    Dx(i,k)=Rx;
    Dy(i,k)=Ry;
    R(i,k)=sqrt(Rx^2+Ry^2);
    alpha(i,k)=atan(Ry/Rx)*180/pi;

    if Rx < 0 && Ry > 0
        alpha(i,k) = alpha(i,k) + 180;
    elseif Rx < 0 && Ry < 0
        alpha(i,k) = alpha(i,k) + 180;
    elseif Rx > 0 && Ry < 0
        alpha(i,k) = alpha(i,k) + 360;
    end

    Alpha = alpha(i,k);
    slotdir = 12:12:360;
    Rslot = find((slotdir < Alpha & slotdir > Alpha-6) | (slotdir > Alpha & slotdir < Alpha+6));
    newGH = length(find(Thetanew==0));
    nearRslots = Rslot*12-3*12:12:Rslot*12+3*12;

    openslots = find(ismember(nearRslots,Thetanew)==0);
    openslotdir = nearRslots(openslots);
```

```
        if length(newGH)>length(openslotdir) && newGH ~=0
            Thetanew = [Thetanew; openslotdir'];
        elseif length(newGH)<length(openslotdir) && newGH ~=0
            slotprob=[ones(length(openslotdir),1).*probr(1)/length(openslotdir);probr(2)];
            for q=1:length(newGH)
                r=rand;
                x = sum(r >= cumsum([0; slotprob]));
                for z=1:length(openslotdir)
                    if z==x
                        Thetanew=[Thetanew; openslotdir(z)];
                    end
                end
            end
        end

        Thetanew(Thetanew==0)=[];
        thetanew=Thetanew./12;
        newThetapos = randperm(30)';
        norepeats=find(ismember(newThetapos,thetanew)==0);
        newThetapos=newThetapos(norepeats);
        if GHr-length(Thetanew) == 0
            Theta = Thetanew;
        else
            T = newThetapos(1:GHr-length(Thetanew)).*12;
            Theta=[Thetanew; T];
        end

    end

    for i=2:t+1

        X(i,k) = Dx(i-1,k)+X(i-1,k);
        Y(i,k) = Dy(i-1,k)+Y(i-1,k);

    end

end

NetDispR = sqrt((X(size(X,1),:)-X(1,:)).^2+(Y(size(Y,1),:)-Y(1,:)).^2);
SpeedR = sum(R,1)/(t*int);

AbsNetAlphar = atan(sum(abs(Dy))./sum(abs(Dx)));

CIr = sqrt((sum(abs(Dx))).^2+(sum(abs(Dy))).^2)./sum(R).*cos(AbsNetAlphar);

Speed = [SpeedA' SpeedR'];
```

CI = [CIa' CIr'];

Supporting References

1. Heck, J. N., S. M. Ponik, M. G. Garcia-Mendoza, C. A. Pehlke, D. R. Inman, K. W. Eliceiri, P. J. Keely. 2012. Microtubules regulate GEF-H1 in response to extracellular matrix stiffness. Mol Biol Cell. 23:2583-2592.
2. Vader, D., A. Kabla, D. Weitz, L. Mahadevan. 2009. Strain-induced alignment in collagen gels. PLoS One. 4:e5902.
3. Chua Chee, K. 1994. Three-dimensional rapid prototyping technologies and key development areas. Computing & Control Engineering Journal. 5:200-206.
4. Wozniak, M. A., P. J. Keely. 2005. Use of three-dimensional collagen gels to study mechanotransduction in T47D breast epithelial cells. Biol Proced Online. 7:144-161.
5. Roeder, B. A., K. Kokini, J. E. Sturgis, J. P. Robinson, S. L. Voytik-Harbin. 2002. Tensile mechanical properties of three-dimensional type I collagen extracellular matrices with varied microstructure. J Biomech Eng. 124:214-222.
6. Lopez-Garcia, M. D., D. J. Beebe, W. C. Crone. 2010. Young's modulus of collagen at slow displacement rates. Biomed Mater Eng. 20:361-369.
7. Sung, K. E., G. Su, C. Pehlke, S. M. Trier, K. W. Eliceiri, P. J. Keely, A. Friedl, D. J. Beebe. 2009. Control of 3-dimensional collagen matrix polymerization for reproducible human mammary fibroblast cell culture in microfluidic devices. Biomaterials. 30:4833-4841.
8. Schindelin, J., I. Arganda-Carreras, E. Frise, V. Kaynig, M. Longair, T. Pietzsch, S. Preibisch, C. Rueden, S. Saalfeld, B. Schmid, J. Y. Tinevez, D. J. White, V. Hartenstein, K. Eliceiri, P. Tomancak, A. Cardona. 2012. Fiji: an open-source platform for biological-image analysis. Nat Methods. 9:676-682.
9. Yeung, T., P. C. Georges, L. A. Flanagan, B. Marg, M. Ortiz, M. Funaki, N. Zahir, W. Ming, V. Weaver, P. A. Janmey. 2005. Effects of substrate stiffness on cell morphology, cytoskeletal structure, and adhesion. Cell Motil Cytoskeleton. 60:24-34.
10. Pelham, R. J., Jr., Y. Wang. 1997. Cell locomotion and focal adhesions are regulated by substrate flexibility. Proc Natl Acad Sci U S A. 94:13661-13665.
11. Aratyn-Schaus, Y., P. W. Oakes, J. Stricker, S. P. Winter, M. L. Gardel. 2010. Preparation of complaint matrices for quantifying cellular contraction. J Vis Exp.
12. Schoen, I., B. L. Pruitt, V. Vogel. 2013. The Yin-Yang of Rigidity Sensing: How Forces and Mechanical Properties Regulate the Cellular Response to Materials. Annual Review of Materials Research. 43:589-618.
13. Smith, A. S., K. Sengupta, S. Goennenwein, U. Seifert, E. Sackmann. 2008. Force-induced growth of adhesion domains is controlled by receptor mobility. Proc Natl Acad Sci U S A. 105:6906-6911.
14. Huttenlocher, A., A. R. Horwitz. 2011. Integrins in cell migration. Cold Spring Harb Perspect Biol. 3:a005074.